JOURNAL OF GUIDANCE, CONTROL, AND DYNAMICS
Vol. 23, No. 3, May–June 2000

Fuel-Optimal Planar Earth–Mars Trajectories Using Low-Thrust Exhaust-Modulated Propulsion

S. R. Vadali* and R. Nah†
Texas A&M University, College Station, Texas 77843-3141
and
E. Braden‡ and I. L. Johnson Jr.‡
NASA Johnson Space Center, Houston, Texas 77058

The determination of fuel-optimal, planar, Earth–Mars trajectories of spacecraft using low-thrust, variable specific impulse I_{sp} propulsion is discussed. The characteristics of a plasma thruster currently being developed for crewed/cargo missions to Mars are used. This device can generate variable I_{sp} within the range of 1000–35,000 s, at constant power. The state equations are written in rotating, polar coordinates, and the trajectory is divided into two phases, patched together at an intermediate point between the Earth and Mars. The gravitational effects of the sun, Earth, and Mars are included in the two phases. The formulation of the problem treats the spacecraft mass as a state variable, thus, coupling the spacecraft design to the trajectory design. The optimal control problem is solved using an indirect, multiple shooting method. Results for a 144-day crewed mission to Mars are presented. The variation of the I_{sp} during spacecraft's escape from the Earth's gravitational field shows an interesting periodic behavior with respect to time. The results obtained are also compared with those obtained by assuming a three-phase trajectory, with the Earth, sun, and Mars, influencing the spacecraft, one per phase, in sequence.

Introduction

MARS is the most accessible planet beyond the Earth–moon system where a sustainable human presence could be maintained. The technology needed to send humans to Mars and sustain them there can inspire new advances in all of the sciences. There is currently considerable interest in developing unconventional propulsion systems that will enable crewed missions to the outer solar system. The idea of using low-thrust propulsion for interplanetary missions has been propounded since the early 1960s.[1] This idea has become a reality with the successful performance of the NSTAR ion thruster on the Deep Space-1 mission launched by NASA in October 1998.

An experimental plasma thruster using compact, high-field, lightweight superconductors has been developed under the direction of Chang-Diaz at the NASA Johnson Space Center (see Ref. 2). When scaled for the mission to Mars, this high-power and low-weight design will have a specific mass of about 6 kg/kW. It uses a neutral gas like hydrogen as a propellant and rf-wave heating for plasma generation. The exhaust mass flow is controlled by using an electromagnetic field. This device can generate variable I_{sp} at constant power. The maximum power required is estimated to be 10 MW. It is estimated that the engine can provide a minimum I_{sp} of 1000 s and a maximum I_{sp} of 35,000 s. The I_{sp} can be varied from the minimum to the maximum and vice versa in 15 min. It is speculated that the magnetic field inside the thruster has the potential to bend the trajectories of the high-energy solar particles, providing a region of reduced radiation.

This paper deals with the computation of fuel-optimal Earth–Mars trajectories utilizing the engine characteristics just mentioned. An example problem of a crewed mission to Mars in the year 2014[3] is considered. It is assumed that previous to this mission a cargo mission will depart in the year 2011 to land surface equipment, fuel facilities, and other necessities to sustain life on Mars. The initial spacecraft mass is estimated to be 525,000 kg. Earth departure is from a 320-km circular parking orbit, and the target is a circular synchronous orbit around Mars [orbit of 6 Mars radii or $6DU_M$ (distance unit with respect to a planet)]. Although the flight duration is chosen to be 144 days, it can be decreased at the expense of fuel. It is assumed in this preliminary study that Earth and Mars are in planar, circular orbits about the sun and that the transfer orbit is also planar. Note that the eccentricity of the orbit of Mars is approximately 0.094. This should be exploited for determining a launch date that requires the least amount of fuel. Furthermore, it is cheaper to establish a polar orbit around Mars in comparison to an equatorial orbit of the same shape and size. These issues have not been dealt with in this paper.

Melbourne[1] developed the concept of power-limited propulsion for interplanetary missions. The performance index used in his work for fuel-optimal control is the integral of the square of the thrust acceleration of the spacecraft. Because spacecraft mass is not used as an explicit state variable, this approach uncouples the trajectory design problem from the spacecraft design problem. Kechichian[4] presents an overview of the literature on optimal low-thrust orbit transfer problems using equinoctial orbit elements as the states. He also treats the minimum-fuel orbit transfer problem with variable, bounded I_{sp} using a penalty function approach. Scheel and Conway[5] solve minimum-time problems for low Earth orbit (LEO) to geosynchronous Earth orbit (GEO) and GEO to outer orbit transfers using the method of collocation and parallel shooting. The effect of Earth's oblateness is included in this study.

Low-thrust heliocentric fuel optimal trajectories for split-sprint Mars missions have been reported in Ref. 2. These missions consist of long duration (180 days) uncrewed cargo missions with up to 66% payload followed by a rapid (90–104 days) crewed trip with a light payload in the range of 2–14% of the spacecraft mass. These estimates of flight times are optimistic because the Earth-escape and Mars-capture portions of the trajectories have not been considered. The formulation presented in Ref. 2 is basically the same as that of Melbourne[1] in that the fuel consumption and the variation in I_{sp} are obtained indirectly after optimization. The actual performance index minimized is the integral of the square of the thrust acceleration. The limits on I_{sp} are not imposed. Similar formulations can also be found in the following references. Coverstone-Carroll and Williams[6] use the method of differential inclusions to solve for optimal low-thrust interplanetary trajectories. Kluever[7] presents a method based on sequential quadratic programming for solving a variety of low-thrust interplanetary trajectory optimization

Received 12 March 1999; revision received 27 September 1999; accepted for publication 2 October 1999.

*Professor, Department of Aerospace Engineering; svadali@tamu.edu. Associate Fellow AIAA.
†Graduate Student, Department of Aerospace Engineering.
‡Aerospace Engineer, EG5/Advanced Mission Design.

problems using the equinoctial elements. Thorne and Hall[8] treat the minimum-time continuous thrust orbit transfer problem and present approximate analytical results for the optimal initial costates to be used in a shooting method.

The following references treat the more complex, interplanetary trajectory optimization problems by including the gravitational influence of multiple bodies. Planar and three-dimensional minimum-fuel lunar trajectories utilizing a combined direct and indirect solution method have been presented by Pierson and Kluever[9] and Kluever and Pierson.[10] In these works, both thrusting and coasting arcs are used, and the thrust is assumed to be constant. Application of collocation and nonlinear programming to the minimum-time Mars-capture problem is presented by Tang and Conway.[11] In Ref. 11, the patched conic equivalent of the low-thrust problem is treated, that is, only one planet is assumed to influence the trajectory during a particular phase. This is a practical approach for solving such a sensitive optimization problem. The thrust acceleration is assumed to be constant in this work; hence, the optimal solution is also fuel minimizing.

An indirect, multiple shooting method is used to solve the optimal control problem posed in this paper. It is well known that this method suffers from extreme sensitivity when applied to complex problems. However, when the method works, it does produce highly accurate solutions and can reveal very fine features of the controls without any need to guess the switching structure. To begin, optimal trajectories are generated for simpler problems, as utilized in Refs. 9–11. A maximum-energy problem for Earth escape and a minimum-fuel problem for the heliocentric phase of the trajectory to the orbit of Mars are solved, separately, in this work. The departure asymptote with respect to the Earth, in the geocentric phase, is arbitrarily set to be along the Earth's velocity vector with respect to the sun. The initial conditions for the heliocentric phase are chosen to be sufficiently far from the Earth. These two solutions are then patched together such that the necessary fuel optimality and continuity conditions are satisfied in the presence of the sun and Earth only. The patch point is typically at 30–40 days from Earth departure. Next, the gravitational effect of Mars is introduced only in the heliocentric phase, and the departure date is adjusted until a fuel optimal trajectory is achieved with a termination point of approximately $300DU_M$ with respect to Mars. Subsequently, circular orbit boundary conditions at $300DU_M$ are imposed to obtain a fuel-optimal capture trajectory. From this point onward, the two phases for the trajectory are computed with the Earth and Mars as reference points. Subsequently, the final capture orbit radius is reduced to $6DU_M$. The process is described in more detail later.

The key features of this paper are the accommodation of the limits on the I_{sp} and the treatment of the jump conditions of the costate variables at the patch point. The results obtained using a continuous gravity field model of the planets are also compared with those obtained by assuming a three-phase trajectory, with the Earth, sun, and Mars influencing the spacecraft, one per phase, in sequence.

System Equations

Two sets of equations are presented, one for the geocentric coordinate system and the other for the heliocentric coordinate system, as shown in Figs. 1 and 2. Most of the variables are shown in Figs. 1

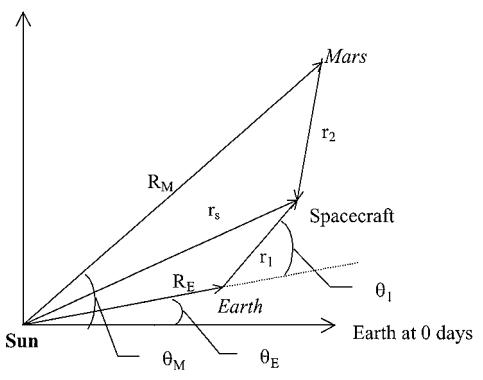

Fig. 1 Geocentric rotating coordinate system.

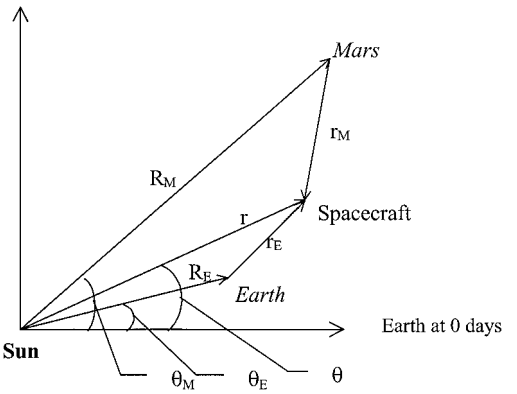

Fig. 2 Heliocentric inertial coordinate system.

and 2. The equations in the geocentric coordinate system can be easily modified to obtain the equations in the areocentric coordinate system. Specifically, the subscripts E and M should be interchanged for this purpose. The gravitational parameters of the various denoted by μ with corresponding subscripts. The efficiency and maximum power required are denoted by ε and P, respectively. The acceleration due to gravity at the Earth's sea level is indicated by g. The control inputs, u_1 and u_2, are functions of I_{sp} and ϕ, the thrust steering angle with respect to the local horizontal:

$$u_1 = \sin\phi / I_{sp} \tag{1}$$

$$u_2 = \cos\phi / I_{sp} \tag{2}$$

Geocentric Coordinate System State Equations

$$\dot{r}_1 = V_{r_1} \tag{3}$$

$$\dot{V}_{r_1} = (1/r_1)\left(V_{\theta_1} + \dot{\theta}_E r_1\right)^2 - \mu_E \left| r_1^2 + \left\{ R_E \dot{\theta}_E^2 \cos\theta_1 - \mu_s (r_1 + R_E \cos\theta_1) \right| r_s^3 - \mu_M [r_1 + R_E \cos\theta_1 - R_M \cos(\theta_1 + \theta_E - \theta_M)] \left| r_2^3 \right\} + (2\varepsilon P / m_1 g) u_1 \tag{4}$$

$$\dot{V}_{\theta_1} = -\left(V_{r_1} V_{\theta_1} \left| r_1\right.\right) - 2\dot{\theta}_E V_{r_1} + \left\{ -R_E \dot{\theta}_E^2 \sin\theta_1 + \mu_s R_E \sin\theta_1 \left| r_s^3 + \mu_M (R_E \sin\theta_1 - R_M \sin(\theta_1 + \theta_E - \theta_M)) \right| r_2^3 \right\} + (2\varepsilon P / m_1 g) u_2 \tag{5}$$

$$\dot{\theta}_1 = V_{\theta_1} \left| r_1 \right. \tag{6}$$

$$\dot{m}_1 = -(2\varepsilon P / g^2)\left(u_1^2 + u_2^2\right) \tag{7}$$

The state variables are as follows: r_1 is the distance of the spacecraft with respect to the center of the Earth, θ_1 is its longitude with respect to the rotating sun–Earth line, V_{r_1} and V_{θ_1} are the radial and transverse components of the velocity in the rotating coordinate system, respectively. The mass of the spacecraft is m_1. The terms within braces in Eqs. (4) and (5) can be neglected inside the sphere of influence of the Earth. A similar approximation can be made inside the sphere of influence of Mars. These approximations give rise to the patched conic equivalent for low-thrust trajectories.[11]

Heliocentric Coordinate System State Equations

These equations are derived in the inertial heliocentric coordinate system shown in Fig. 2. There is a slight change in notation, which should be clear from Fig. 2. Here we use m for the mass of the spacecraft, r for its distance with respect to the sun, and θ for its longitude with respect to the sun–Earth line at the beginning of the mission:

$$\dot{r} = V_r \tag{8}$$

$$\dot{V}_r = V_\theta^2 \left| r - \mu_s \right| r^2 - \left\{ \mu_E [r - R_E \cos(\theta - \theta_E)] \left| r_E^3 + \mu_M [r - R_M \cos(\theta - \theta_M)] \right| r_M^3 \right\} + (2\varepsilon P / mg) u_1 \tag{9}$$

$$\dot{V}_\theta = -(V_r V_\theta / r) - \left\{ \mu_E R_E \sin(\theta - \theta_E) \middle| \; r_E^3 \right.$$
$$\left. + \mu_M R_M \sin(\theta - \theta_M) \middle| \; r_M^3 \right\} + (2\varepsilon P / mg) u_2 \tag{10}$$

$$\dot{\theta} = V_\theta / r \tag{11}$$

$$\dot{m} = -(2\varepsilon P / g^2)\left(u_1^2 + u_2^2\right) \tag{12}$$

The terms inside braces in Eqs. (9) and (10) are the perturbations due to the Earth and Mars. These terms are negligible during the heliocentric portion of the trajectory. The effect of these approximations will be discussed later.

Optimal Control Problem

It is desired to deliver the spacecraft from a low-altitude, circular, Earth orbit and minimize the fuel expended or maximize the final mass of the spacecraft at insertion into a circular orbit about Mars. Hence, the performance optimization function is written as

$$\text{minimize: } J = -m_1(t_f) \tag{13}$$

The constraints are Eqs. (3–7), for the geocentric phase and the corresponding equations for the areocentric phase, and Eqs. (8–12), for the heliocentric phase and boundary conditions at Earth departure and Mars arrival. In addition to these constraints, the minimum and maximum I_{sp} constraints must be imposed:

$$I_{sp_{min}} \le 1 \Big| \sqrt{u_1^2 + u_2^2} \le I_{sp_{max}} \tag{14}$$

Furthermore, at the patch point where the reference central body is switched, the necessary jump conditions on the costates must be satisfied. The initial longitude at Earth departure and the final longitude at Mars arrival are free to be selected.

As mentioned in the Introduction, this problem has to be solved in steps, starting from feasible solutions or optimal solutions to simpler problems. One such problem is the maximum-energy escape from the Earth. This performance optimization function for this problem is written as

$$\text{minimize: } J = -\tfrac{1}{2}\left[V_{r_1}^2(t_f) + V_{\theta_1}^2(t_f) \right] + \mu_E / r_1(t_f) \tag{15}$$

The state equations used for this problem are Eqs. (3–7), with the influence of Mars switched off.

The control Hamiltonian for the geocentric/areocentric trajectory is written as

$$H = \lambda_{r_1} \dot{r}_1 + \lambda_{V_{r_1}} \dot{V}_{r_1} + \lambda_{V_{\theta_1}} \dot{V}_{\theta_1} + \lambda_{\theta_1} \dot{\theta}_1 + \lambda_{m_1} \dot{m}_1 \tag{16}$$

where the λ are the costates. The costate equations can be derived using optimal control formalism,[12] for example,

$$\dot{\lambda}_{r_1} = -\frac{\partial H}{\partial r_1} \tag{17}$$

The optimal controls are determined using Pontryagin's principle to minimize the Hamiltonian. If the controls are unconstrained, the optimality condition can be written as

$$\frac{\partial H}{\partial u_1} = 0, \qquad i = 1, 2 \tag{18}$$

Regardless of the performance index [Eq. (13) or (15)], the costate equations as well as the control logic remain the same. Various forms of the control logic are presented in the Appendix. The costate equations can be found in Ref. 13. Note that the form of the Hamiltonian will still be the same as given earlier, when the central body is switched, that is, Earth and Mars are interchanged.

Initial, Boundary, and Jump Conditions

The initial and boundary conditions for the minimum-fuel problem are given next.

Boundary Conditions at t_0

With free $\theta_1(t_0)$,

$$r_1(t_0) = r_0 \tag{19}$$

$$V_{r_1}(t_0) = 0 \tag{20}$$

$$V_{\theta_1}(t_0) = \sqrt{\mu_E / r_0} - \dot{\theta}_E r_0 \tag{21}$$

$$\lambda_{\theta_1}(t_0) = 0 \tag{22}$$

$$m_1(t_0) = m_0 \tag{23}$$

Equation (22) is a transversality condition that arises because $\theta_1(t_0)$ is free.

Boundary Conditions at t_f

With free $\theta_1(t_f)$ and $m_1(t_f)$,

$$r_1(t_f) = r_f \tag{24}$$

$$V_{r_1}(t_f) = 0 \tag{25}$$

$$V_{\theta_1}(t_f) = \sqrt{\mu_M / r_f} - \dot{\theta}_M r_f \tag{26}$$

$$\lambda_{\theta_1}(t_f) = 0 \tag{27}$$

$$\lambda_{m_1}(t_f) = -1 \tag{28}$$

Equations (27) and (28) are transversality conditions that arise due to $\theta_1(t_f)$ and $m_1(t_f)$ being free.

Jump Conditions at the Patch Point t_{int}

The jump conditions for switching between the Earth and the sun are of interest. These conditions are also applicable to switching between Mars and the sun by changing the subscript E to M. The time from Earth departure at which the central body is switched is selected somewhat arbitrarily. Hence, it is not a free variable to be optimized. The constraints at the patch point are continuity in radial and angular positions, radial and transverse velocities, and the mass of the spacecraft. Symbolically, these conditions are written as $\Psi[\boldsymbol{x}(t_{int}^-), \boldsymbol{x}(t_{int}^+)] = 0$, where $\boldsymbol{x}$ is the state vector. These conditions are shown in detail in the Appendix. The intermediate point constraints are augmented to the performance index via a Lagrange multiplier vector $\boldsymbol{\nu}$. The jump conditions[12] are

$$\Psi_{\boldsymbol{x}}^T \Big|_{t_{int}^-} \boldsymbol{\nu} - \boldsymbol{\lambda}\left(t_{int}^-\right) = 0 \tag{29}$$

$$\Psi_{\boldsymbol{x}}^T \Big|_{t_{int}^+} \boldsymbol{\nu} - \boldsymbol{\lambda}\left(t_{int}^+\right) = 0 \tag{30}$$

where $\boldsymbol{\lambda}$ is the vector of costates and $\Psi_{\boldsymbol{x}}$ is the Jacobian of Ψ, which is square and nonsingular. The superscripts $+$ and $-$|, denote instances just after and just before t_{int}, respectively. Either of the two equations can be used to eliminate $\boldsymbol{\nu}$ and to obtain the following jump conditions for the costates:

$$\boldsymbol{\lambda}\left(t_{int}^+\right) + \Psi_{x_{t_{int}^+}}^{T} \Psi_{x_{t_{int}^-}}^{-T} \boldsymbol{\lambda}\left(t_{int}^-\right) = 0 \tag{31}$$

Elimination of the Lagrange multipliers reduces the number of unknowns that have to be determined.

Spacecraft and Trajectory Data

Most of the data used in this paper are obtained from Ref. 3. The estimate of the initial mass of the spacecraft is 525,000 kg. The required power is 10 MW, and the engine efficiency is 0.6. The specific mass of the spacecraft is 6 kg/kW. The minimum and maximum I_{sp} values are 1000 and 35,000 s, respectively. The specified payload mass is 35,000 kg, and the powerplant mass is 60,000 kg. Hence, any final mass above 95,000 kg can be used for additional payload or reserve fuel that can be used in the return mission. Alternatively, the flight time could be reduced. The initial mass of 525,000 kg was estimated using a baseline Earth–Mars transfer with a fuel-optimal heliocentric phase and Earth-escape and Mars-capture phases with

constant I_{sp} of 1000 s. The initial circular orbit altitude is 320 km ($1.05DU_E$), and the final Martian orbit is circular with a radius of $6DU_M$. The parking orbit altitude at Earth is lower than that considered in Ref. 3. The trip time is fixed at 144 days.

Method of Solution

The initial, terminal, and intermediate point constraints are treated as nonlinear algebraic functions of the unknowns to be determined. The constraints are evaluated using the state, costate, and control equations. This problem is solved using a modified Newton's method with step size control (H. Sywald, private communication, 1994). The differential equations are integrated using a Runge–Kutta-Fehlberg seventh-order scheme with an accuracy of 10 digits. The constraints are assumed to be satisfied if the constraint norm is less than 10^{-10}. Appropriate canonical units are used for time, position, and velocity variables.[14] The sequence of problems that was solved to achieve the final objective is given as follows.

1) For Earth escape with maximum-energy, the gravitational effect of the sun was included. The departure asymptote with respect to the Earth was constrained to be along the Earth's velocity vector with respect to the sun, that is, $\theta_1(t_f) = 90$ deg. The initial value of the longitude was left free, and the final time was set in the range of 25–40 days.

2) A heliocentric minimum-fuel trajectory from Earth's orbit to that of Mars was computed by including the Earth's gravitational effect but not that of Mars. The departure point with respect to the Earth was chosen to avoid extreme sensitivity of the trajectory to Earth's gravity. The departure longitude was set to zero, but the longitude at arrival was left free. The final time was in the range of 104–119 days.

3) For a minimum-fuel trajectory from LEO to the orbit of Mars, initial guesses for the unknown quantities were obtained from the solutions to problems 1 and 2. Minimum-fuel necessary conditions as well as continuity of the variables at the patch point were enforced. The initial and final longitudes were treated as free variables. The geocentric phase of the trajectory was integrated forward, and the heliocentric trajectory was integrated backward in time from the orbit of Mars.

4) For problem 3 with the effect of Mars included in the heliocentric phase, the initial phase angle of Mars with respect to the Earth (or Earth departure date) was adjusted so that the spacecraft was $300DU_M$ from Mars at the final time. Subsequently, circular orbit conditions at $300DU_M$, were imposed with respect to Mars.

5) For the minimum-fuel problem using two phases, geocentric phase and areocentric phase for a $300DU_M$ circular orbit, the gravitational effect of Mars was included in both the phases of the trajectory. The jump conditions and the constraints were evaluated at the patch point by using an Earth–sun transformation and a Mars–sun transformation of the states. The constraint errors were evaluated in heliocentric canonical units.

6) Reduce the final circular orbit radius. The final orbit radius was reduced to $6.5DU_M$ but could not be reduced further due to sensitivity problems. However, it was found that the problem is less sensitive if the final longitude is treated as fixed. The final longitude $\theta_1(t_f)$ was fixed at approximately 180 deg, a value obtained from a previously converged solution, and the final radius was decreased to $6DU_M$. Next, the Mars–Earth phase angle at Earth departure was adjusted until the boundary condition $\lambda_{\theta_1}(t_f) = 0$ was approximately satisfied. This solution was used in the free-longitude problem to obtain the final solution.

Multiple Extremal Solutions

The first solution obtained for the free-$\theta_1(t_f)$ optimal control problem was compared against neighboring solutions obtained by solving a few fixed-$\theta_1(t_f)$ optimal control problems. The values of $\theta_1(t_f)$ were chosen to bracket that obtained from the free-longitude solution. It was found that the neighboring fixed-$\theta_1(t_f)$ solutions were more optimal than the free-$\theta_1(t_f)$ solution. The final spacecraft mass predicted by the free-$\theta_1(t_f)$ solution was indeed found to be a local minimum instead of a local maximum, with respect to $\theta_1(t_f)$. The variation in the costate $\lambda_{\theta_1}(t_f)$ also confirmed the same conclusion. Then a series of problems with various fixed values of $\theta_1(t_f)$ in the range of π–2π were solved to determine approximately the minimum of the cost function. This feasible solution was used to obtain another extremal solution for the free-longitude problem with a lower cost than previously obtained. Using this procedure, two extremal solutions were obtained for many of the examples considered during the course of this work.

Results

The fuel-optimal solution to the $6DU_M$ target circular orbit around Mars, including the effects of the Earth, Mars, and sun is shown in Figs. 3a–3c. The trip time is 144 days, and the Earth-Mars phase angle at departure is 36 deg, that is, Mars leads Earth by this amount. The patch point is at 72 days from departure. Figure 3a shows the Earth-escape spiral on a polar plot. Note that this depiction is in the rotating, geocentric coordinate system, that the radius scale in Fig. 3a is in terms of DU_E, and that the angle variable is θ_1. The radius vector from the Earth to the sun is inclined at 180 deg. The spacecraft makes approximately 131 revolutions around the Earth before escaping. The time for escape is approximately 30 days from Earth departure. The escape asymptote is inclined nearly 30 deg with respect to the sun–Earth line. Figure 3b shows the entire trajectory in the heliocentric, inertial coordinate system. The radius scale in the polar plot is in terms of astronomical units, and the angle variable is θ. Figure 3c shows the Mars-capture spiral in the areocentric, rotating coordinate system, from which it can be seen that the spacecraft completes nearly 1.5 revolutions before establishing the final orbit. The radius scale in Fig. 3c is in terms of DU_M. The final longitude of the spacecraft is 340.34 deg with respect to the sun–Mars line. The number of revolutions the spacecraft makes for Mars capture is significantly less than that for Earth escape because the thrust acceleration levels are much higher near Mars than near the Earth and the gravity field of Mars is weaker than that of the Earth. Furthermore, the radius at Earth departure is $1.05DU_E$, whereas Mars arrival radius is $6DU_M$. At the beginning of the trajectory, with minimum I_{sp}, the thrust acceleration level is approximately $2.37 \times 10^{-4}\ g$, whereas, near the end of the trajectory, with minimum I_{sp}, the thrust acceleration is of the order of $10^{-3}\ g$.

Figure 4 shows the thrust steering angle that is measured with respect to the local horizontal. The segment from 0–72 days is with respect to the geocentric, rotating reference frame, and the subsequent segment is shown in the areocentric, rotating reference frame. These results are similar to those presented in Ref. 11. The variation of I_{sp} with respect to time is shown in Fig. 5a. Figure 5a shows that the thrust is modulated near the end of the Earth-escape phase to nudge the spacecraft away from the pull of the Earth. A cross plot of I_{sp} vs the longitude with respect to the sun–Earth line θ_1 for a period of 30 days is shown in Fig. 5b. It can be seen from Fig. 5b that the peaks in the I_{sp} plots occur at $\theta_1 = 90$ deg, that is, when the spacecraft is located along the velocity vector of the Earth with respect to the sun. Higher I_{sp} is equivalent to lower thrust, which leads to lower fuel consumption. Figure 6 shows the variation in the mass of the vehicle. The final mass of the spacecraft is 127,331 kg. This figure of merit should be compared with 95,000 kg, which is the spacecraft mass without any fuel, as estimated in Ref. 3.

Battin[15] presents a formula for the number of revolutions required to escape a planet using a small constant tangential acceleration. To use this formula, the average values of I_{sp} and mass over the first 30 days are calculated from the results obtained, as 1081 s and 366,991 kg, respectively. Even though the thrust is not exactly tangential over this period, it is nearly so for a substantial part. With these values, the number of revolutions predicted by Battin's formula is 114.5 as compared to 131 revolutions for the optimal solution presented. Similarly, when applied to the capture phase of the trajectory (estimated to occur during the last 7 days), based on an average I_{sp} of 2520 s and mass of 135,289 kg, the number of revolutions predicted is approximately 1, where as the optimal solution has nearly 1.5 revolutions.

A parametric study was undertaken with the initial Earth–Mars phase angle as a variable. Figure 7 shows the variation of the final

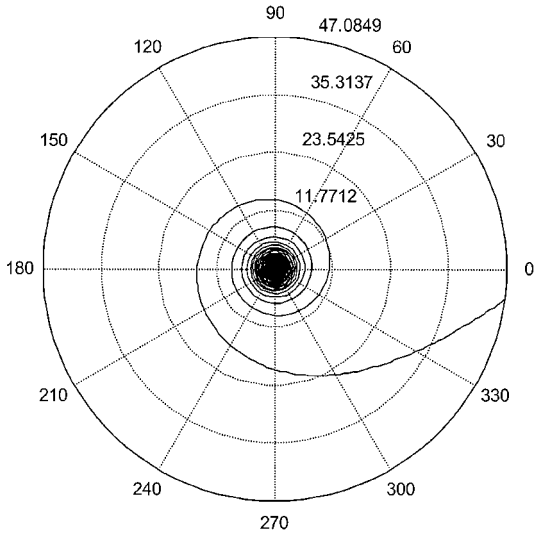

Fig. 3a Minimum-fuel trajectory for 0–25 days, rotating geocentric coordinate system (radius in DU_E).

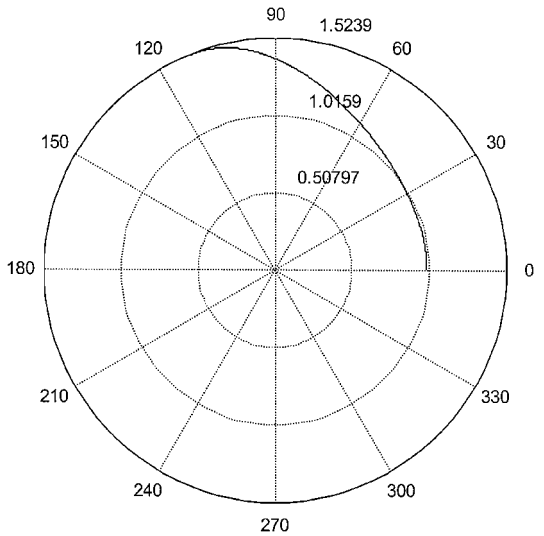

Fig. 3b Minimum-fuel trajectory in the heliocentric inertial coordinate system (radius in astronomical units).

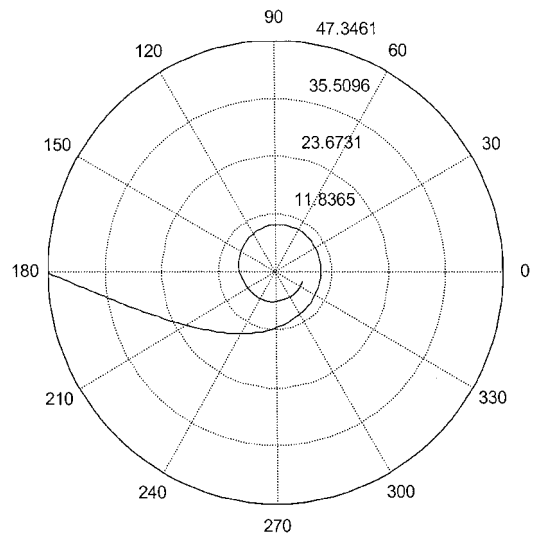

Fig. 3c Minimum-fuel trajectory for 132–144 days, rotating areocentric coordinate system (radius in DU_M).

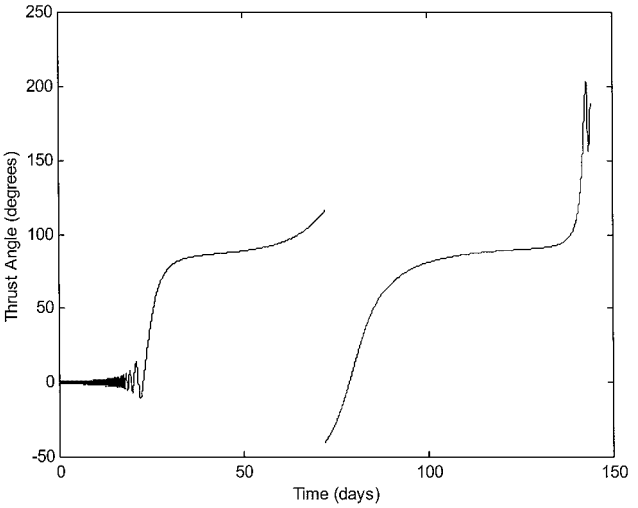

Fig. 4 Variation of the thrust angle with respect to the local horizontal (0–72 days in geocentric system, 72–144 days in areocentric system).

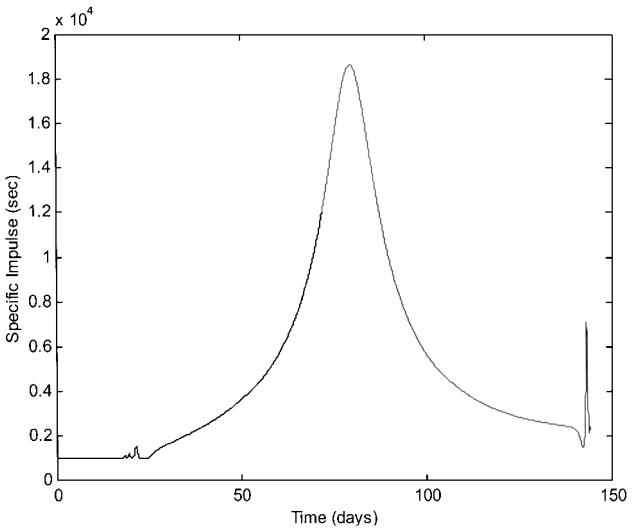

Fig. 5a Variation of the I_{sp} with respect to time.

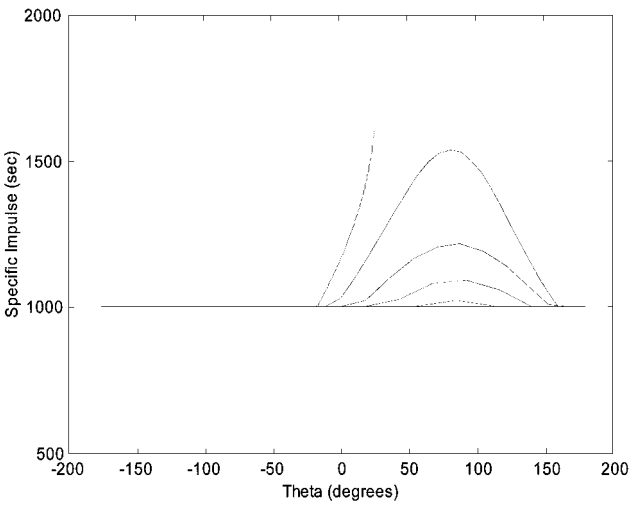

Fig. 5b I_{sp} vs sun–Earth longitude (0–30 days).

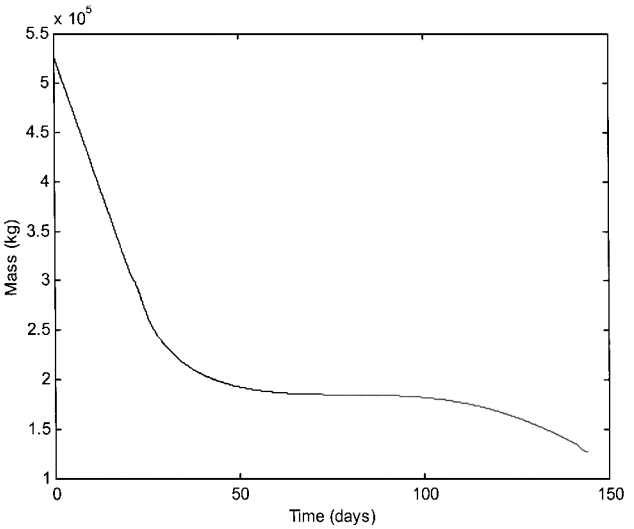

Fig. 6 Variation of the spacecraft mass.

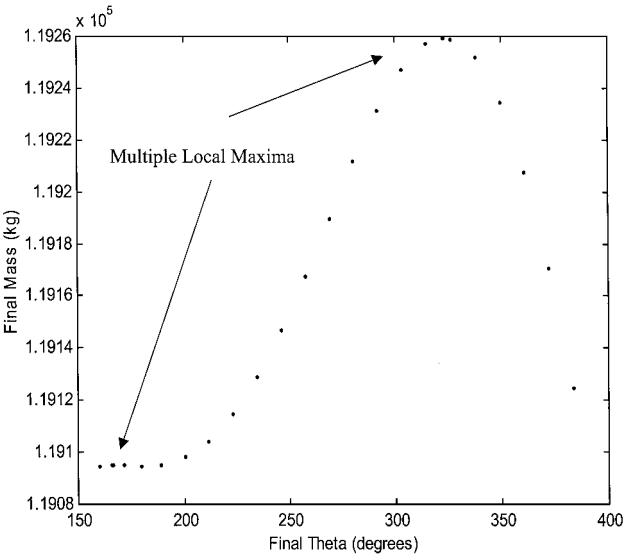

Fig. 8 Final mass vs final sun–Mars longitude.

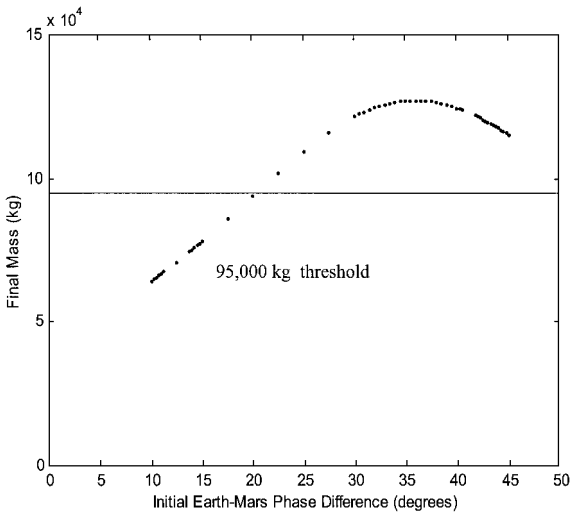

Fig. 7 Final spacecraft mass vs initial Earth–Mars phase angle.

mass as a function of the initial Earth–Mars phase angle. The maximum final mass corresponds to a phase angle of 36 deg, which corresponds to a departure date close to 31 January 2014. From these data, it is seen that some time near the end of January 2014 is a good date for travel if a trip time of 144 days is acceptable. Additionally, it is seen that some of the solutions obtained are infeasible because the final mass is below 95,000 kg.

The multimodal nature of the variation in the final spacecraft mass is shown in Fig. 8. Figure 8 was obtained by solving a number of fixed final-longitude, fuel-optimal control problems. The Earth–Mars phase angle was fixed at 43.25 deg (not 36 deg). A final longitude of 180° corresponds to the transfer orbit terminating between Mars and the sun, on the sun–Mars line. It is clear from Fig. 8 that three local extrema exist for this example. The solution corresponding to the lower local maximum has a final longitude of 163°. The higher local maximum corresponds to a final longitude of 323°. The trajectories corresponding to the two solutions are very similar except near the end. The difference in the final spacecraft mass between the two local maxima is about 160 kg. Because the values for the final mass of the spacecraft shown in Fig. 8 are of the order of 119,000 kg, the difference between the two solutions is of no practical significance.

The results discussed were obtained using the continuous gravity model given in Eqs. (4), (5), (9), and (10). A three-phase discontinuous gravity model was also employed to obtain an approximate solution to the example considered above, with the initial phase angle of Mars set at 36 deg. This model assumes that the first phase (0–30 days) of the trajectory evolves under the gravitational influence of the Earth only. The heliocentric phase lasts from 30 to 137 days during which the sun is the only attracting body. Mars is the only attracting body during the third phase lasting from 137 to 144 days. These approximations were achieved by dropping the terms inside the braces in Eqs. (4), (5), (9), and (10). The optimal control problem was solved using two patch points, one at 30 days and the other at 137 days from the beginning of the mission. The value of the final spacecraft mass predicted by the discontinuous gravitational model was more optimistic than the continuous model by 648 kg. This corresponds to a difference of approximately 0.5%. The number of peaks visible in the plot of I_{sp} vs time in the Earth-escape phase was seven as compared to four (see Fig. 5b) for the continuous model.

Conclusions

Fuel-optimal trajectories for rockets powered by low-thrust propulsion with variable specific impulse are treated. The optimal control problem is solved using an indirect, multiple shooting method. The trajectory is divided into two phases, patched together at an intermediate point between the Earth and Mars. The gravitational effects of the sun, Earth, and Mars are included in the two phases. The formulation of the problem treats the spacecraft mass as a state variable. The optimal I_{sp} variation near the time of Earth escape shows an interesting correlation with the longitude with respect to the sun–Earth line. The optimality of the solutions is investigated using neighboring extremals. It is observed that multiple extrema do occur for this problem with minor differences in the performance index of the order of 100–200 kg. The optimal control problem was also solved using a discontinuous gravitational field model as employed for patched conic analyses. The prediction for the final spacecraft mass, for the same boundary conditions, was 0.5% more optimistic than that obtained using the continuous gravitational model. The results obtained in this paper may in general be optimistic because of the assumptions made regarding the orbit of Mars and the planar trajectories considered.

Appendix: Control Logic and Constraints

Control Logic

The I_{sp} and the thrust steering angle are related to the control variables as

$$I_{sp} = 1 \Big| \sqrt{u_1^2 + u_2^2} \tag{A1}$$

$$\phi = \tan^{-1}(u_1/u_2) \tag{A2}$$

A part of the control Hamiltonian that is of interest here for the application of Pontryagin's principle is

$$\bar{H} = \begin{Bmatrix} \lambda_{V_r} & \lambda_{V_\theta} \end{Bmatrix} \begin{Bmatrix} u_1 \\ u_2 \end{Bmatrix} - \frac{m}{g}\lambda_m \left(u_1^2 + u_2^2\right) \tag{A3}$$

It can be seen that the Hamiltonian is quadratic in the controls. To minimize the preceding expression with respect to the controls, the sign of u_1 should be chosen opposite to that of λ_{V_r} and the sign of u_2 should be opposite to that of λ_{V_θ}. The unconstrained optimal controls are obtained as follows:

$$u_1 = (g/2m)\left(\lambda_{V_r}/\lambda_m\right) \tag{A4}$$

$$u_2 = (g/2m)\left(\lambda_{V_\theta}/\lambda_m\right) \tag{A5}$$

The convexity conditions are

$$\frac{\partial^2 \bar{H}}{\partial u_1^2} = -\frac{4\varepsilon P}{g^2}\lambda_m > 0 \tag{A6}$$

$$\frac{\partial^2 \bar{H}}{\partial u_2^2} = -\frac{4\varepsilon P}{g^2}\lambda_m > 0 \tag{A7}$$

Hence, the solution as just obtained is optimal if $\lambda_m < 0$ and the I_{sp} constraint is not violated.

For a minimum-fuel problem, λ_m is always negative as long as the final time is not too restrictive. However, for a maximum-energy escape problem, λ_m is usually positive. Therefore, additional conditions have to be considered.

For $\lambda_m > 0$, the optimal solution requires minimum I_{sp} or $\sqrt{(u_1^2 + u_2^2)} = 1/I_{sp_{min}}$. This solution is

$$\begin{Bmatrix} u_1 \\ u_2 \end{Bmatrix} = -\frac{1}{I_{sp_{min}}\sqrt{\lambda_{V_r}^2 + \lambda_{V_\theta}^2}} \begin{Bmatrix} \lambda_{V_r} \\ \lambda_{V_\theta} \end{Bmatrix} \tag{A8}$$

For $\lambda_m < 0$, there are two possibilities. If the unconstrained solution is such that $I_{sp} > I_{sp_{max}}$ then the controls are

$$\begin{Bmatrix} u_1 \\ u_2 \end{Bmatrix} = \frac{1}{I_{sp_{max}}\sqrt{\lambda_{V_r}^2 + \lambda_{V_\theta}^2}} \begin{Bmatrix} \lambda_{V_r} \\ \lambda_{V_\theta} \end{Bmatrix} \tag{A9}$$

If the unconstrained solution is such that $I_{sp} < I_{sp_{min}}$, then the controls are the same as in Eq. (A8). The control logic for the case of $\lambda_m < 0$ is similar to that treated in Ref. 4.

Constraints at an Intermediate Point

The requirements of continuity in position and velocity of the spacecraft when the center of the coordinate system is switched from the Earth to the sun (applicable for Mars–sun transformation with minor modifications) give rise to the following equations:

$$\begin{Bmatrix} r \\ 0 \end{Bmatrix} = \begin{bmatrix} \cos(\theta_1 - \theta + \theta_E) & -\sin(\theta_1 - \theta + \theta_E) \\ \sin(\theta_1 - \theta + \theta_E) & \cos(\theta_1 - \theta + \theta_E) \end{bmatrix} \begin{Bmatrix} r_1 + R_E \cos\theta_1 \\ -R_E \sin\theta_1 \end{Bmatrix} \tag{A10}$$

$$\begin{Bmatrix} V_r \\ V_\theta \end{Bmatrix} = \begin{bmatrix} \cos(\theta_1 - \theta + \theta_E) & -\sin(\theta_1 - \theta + \theta_E) \\ \sin(\theta_1 - \theta + \theta_E) & \cos(\theta_1 - \theta + \theta_E) \end{bmatrix} \times \begin{Bmatrix} V_{r1} + R_E\dot{\theta}_E \sin\theta_1 \\ V_{\theta 1} + \dot{\theta}_E(r_1 + R_E\cos\theta_1) \end{Bmatrix} \tag{A11}$$

From these equations, the following constraints are derived:

$$\Psi_1 = r - K_1[r_1\cos(\theta_1 - \theta + \theta_E) + R_E\cos(\theta - \theta_E)]$$

$$\Psi_2 = r_1\sin(\theta_1 - \theta + \theta_E) - R_E\sin(\theta - \theta_E)$$

$$\Psi_3 = V_r - K_2\left[V_{r_1}\cos(\theta_1 - \theta + \theta_E) - \left(V_{\theta_1} + \dot{\theta}_E r_1\right)\sin(\theta_1 - \theta + \theta_E) + R_E\dot{\theta}_E\sin(\theta - \theta_E)\right]$$

$$\Psi_4 = V_\theta - K_2\left[V_{r_1}\sin(\theta_1 - \theta + \theta_E) + \left(V_{\theta_1} + \dot{\theta}_E r_1\right)\cos(\theta_1 - \theta + \theta_E) + R_E\dot{\theta}_E\cos(\theta - \theta_E)\right]$$

$$\Psi_5 = m - m_1 \tag{A12}$$

These constraints for position are evaluated in terms of astronomical unit (AU) and the velocity constraints are evaluated in terms of AU/TU_s, where TU_s is the heliocentric canonical time unit. R_E and r_1 are in the units of DU_E. The canonical unit of time in the geocentric phase is denoted by TU_E. Hence, $K_1 = DU/AU$ and $K_2 = (DU_E/TU_E)$ (TU_s/AU). Note that the same set of equations can be used for the Mars–sun transformation by interchanging Earth and Mars.

Acknowledgments

We thank Hans Seywald of Analytical Mechanics Associates for providing the software used for this work. Discussions with B. Cockrell of NASA Johnson Space Center have been extremely helpful. The suggestions of the reviewers are gratefully acknowledged. Presented as Paper 99-0132 at the AAS/AIAA Space Flight Mechanics Conferences, Breckenridge, CO, 7–10 February 1999.

References

[1] Melbourne, W. G., "Interplanetary Trajectories and Payload Capabilities of Advanced Propulsion Vehicles," Jet Propulsion Lab. TR 32-68, California Inst. of Technology, Pasadena, CA, March 1961.

[2] Chang-Diaz, F. R., Hsu, M. M., Braden, E., Johnson, I., and Yang, T. F., "Rapid Mars Transits with Exhaust Modulated Plasma Propulsion," NASA TP 3539, March 1995.

[3] Sheppard, J., Broome, J., Johnson, I., and Braden, E., "Power-Limited Human Mission to Mars," NASA Johnson Space Center Rept. 28436, Sept. 1998.

[4] Kechichian, J. A., "Optimal Low-Thrust Orbit Transfer," *Orbital Mechanics*, 2nd ed., edited by V. A. Chobotov, AIAA, Reston, VA, 1996, Chap. 14.

[5] Scheel, W., and Conway, B. A., "Optimization of Very-Low-Thrust, Many-Revolution Spacecraft Trajectories," *Journal of Guidance, Control, and Dynamics*, Vol. 17, No. 6, 1994, pp. 1185–1192.

[6] Coverstone-Carroll, V., and Williams, S. N., "Optimal Low Thrust Trajectories Using Differential Inclusion Concepts," *Journal of Astronautical Sciences*, Vol. 42, No. 4, 1994, pp. 379–394.

[7] Kluever, C. A., "Optimal Low-Thrust Interplanetary Trajectories by Direct Method Techniques," *Journal of Astronautical Sciences,* Vol. 45, No. 3, 1997, pp. 247–262.

[8] Thorne, J. D., and Hall, C. D., "Minimum-Time Continuous-Thrust Orbit Transfers," *Journal of Astronautical Sciences*, Vol. 45, No. 4, 1997, pp. 411–432.

[9] Pierson, B. L., and Kluever, C. A., "Three-Stage Approach to Optimal Low-Thrust Earth–Moon Trajectories," *Journal of Guidance, Control, and Dynamics*, Vol. 17, No. 6, 1994, pp. 1275–1282.

[10] Kluever, C. A., and Pierson, B. L., "Optimal Low-Thrust Three-Dimensional Earth–Moon Trajectories," *Journal of Guidance, Control, and Dynamics*, Vol. 18, No. 4, 1995, pp. 817–823.

[11] Tang, S., and Conway, B. A., "Optimization of Low-Thrust Interplanetary Trajectories Using Collocation and Nonlinear Programming," *Journal of Guidance, Control, and Dynamics*, Vol. 18, No. 3, 1995, pp. 599–604.

[12] Bryson, A. E., and Ho, Y.-G., *Applied Optimal Control*, Hemisphere, Washington, DC, 1975, pp. 65, 66, 101–109.

[13] Vadali, S. R., Nah, R., Braden, E., and Johnson, I. L., "Fuel-Optimal Planar Interplanetary Trajectories Using Low-Thrust Exhaust-Modulated Propulsion," American Astronomical Society, Paper 99-132, 7–10 Feb. 1999.

[14] Bate, R. R., Mueller, D. D., and White, J. E., *Fundamentals of Astrodynamics*, Dover, New York, 1971, p. 429.

[15] Battin, R. H., *An Introduction to the Mathematics and Methods of Astrodynamics*, AIAA, New York, 1987, pp. 416, 417.